

See discussions, stats, and author profiles for this publication at: <https://www.researchgate.net/publication/283550441>

# Prediction of Electronically Nonadiabatic Decomposition Mechanisms of Isolated Gas Phase Nitrogen–Rich Energetic Salt: Guanidium–Triazolate

ARTICLE · NOVEMBER 2015

DOI: 10.1016/j.chemphys.2015.10.016

---

READS

34

## 2 AUTHORS:



Jayanta Ghosh

Indian Institute of Science

2 PUBLICATIONS 1 CITATION

[SEE PROFILE](#)

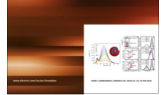


Atanu Bhattacharya

Indian Institute of Science

20 PUBLICATIONS 276 CITATIONS

[SEE PROFILE](#)



# Prediction of electronically nonadiabatic decomposition mechanisms of isolated gas phase nitrogen-rich energetic salt: Guanidium-triazolate



Jayanta Ghosh, Atanu Bhattacharya \*

*Department of Inorganic and Physical Chemistry, Indian Institute of Science, Bangalore 560012, India*

## ARTICLE INFO

### Article history:

Received 3 August 2015

In final form 30 October 2015

Available online 6 November 2015

### Keywords:

Electronically nonadiabatic decomposition

Computational chemistry

Energetic salts

Conical intersections

Electronically excited states

CASSCF, CASPT2, CASMP2 calculations

## ABSTRACT

Electronically nonadiabatic decomposition pathways of guanidium triazolate are explored theoretically. Nonadiabatically coupled potential energy surfaces are explored at the complete active space self-consistent field (CASSCF) level of theory. For better estimation of energies complete active space second order perturbation theories (CASPT2 and CASMP2) are also employed. Density functional theory (DFT) with B3LYP functional and MP2 level of theory are used to explore subsequent ground state decomposition pathways. In comparison with all possible stable decomposition products (such as, N<sub>2</sub>, NH<sub>3</sub>, HNC, HCN, NH<sub>2</sub>CN and CH<sub>3</sub>NC), only NH<sub>3</sub> (with NH<sub>2</sub>CN) and N<sub>2</sub> are predicted to be energetically most accessible initial decomposition products. Furthermore, different conical intersections between the S<sub>1</sub> and S<sub>0</sub> surfaces, which are computed at the CASSCF(14,10)/6-31G(d) level of theory, are found to play an essential role in the excited state deactivation process of guanidium triazolate. This is the first report on the electronically nonadiabatic decomposition mechanisms of isolated guanidium triazolate salt.

© 2015 Elsevier B.V. All rights reserved.

## 1. Introduction

One of the most recent developments in the field of high energy density materials is high nitrogen content energetic salts [1–11]. Salt-based energetic materials often possess advantages over nonionic molecules, as these salts tend to exhibit lower vapor pressure and higher thermal stability than their atomically similar nonionic analogues. They often exhibit strong hydrogen bonds, which result in remarkable stability and considerable insensitivity to physical stimuli, without much altering explosive performance. Furthermore, high energy propellant and explosive properties of energetic salts can be improved and optimized through judicious combination of different anions and cations. However, to improve and control propellant and explosive properties of energetic salts, it is essential to elucidate atomistic mechanisms of their decomposition reactions, which ultimately determine efficient release of stored chemical energy.

Ultimate release of the stored energy during detonation of any energetic material, which finally manifests explosion, definitely depends on phase. True energetic (explosive) behavior is typically displayed only in the condensed phase; an isolated gas phase cluster or molecule does definitely not explode. Nonetheless, the rapid

decomposition process (which, in turn, releases stored energy) of energetic materials must be of molecular in nature prior to any intermolecular chain reaction that can occur in the condensed phase. Therefore, studying the unimolecular decomposition behavior of isolated energetic molecules or clusters (including energetic salt) in the gas phase is an important pursuit both experimentally and theoretically, if we want to understand and design them at a fundamental level.

Guanidium cation and triazolate anion are frequently found as nitrogen rich building block pair in many novel energetic salts [12]. Some of the known guanidium-triazolate-based energetic salts include bis-(triaminoguanidinium) 3,3'-dinitro-5,5'-azo-1,2,4-triazolate (TAGDNAT), triaminoguanidium-(3,3'-dinitroazoxy-1,2,4-triazolate) (TAGDNATO). Chemical structures of these energetic salts are illustrated in Fig. 1. These salts are found to be intrinsically non-volatile and thermally stable under normal conditions and are denser than atomically similar nonionic analogues. Understanding unimolecular decomposition reaction mechanisms of these ionic salts is an important task. However, these molecules are large and may exhibit complex decomposition reaction channels. This is why, taking reductionist approach in the present study, we have selected a structurally simple analogue salt, guanidium triazolate (see Fig. 1 for chemical structure), which can arguably serve as a model system for the entire class of guanidium triazolate-based energetic salts.

\* Corresponding author.

E-mail address: [atanub@ipc.iisc.ernet.in](mailto:atanub@ipc.iisc.ernet.in) (A. Bhattacharya).

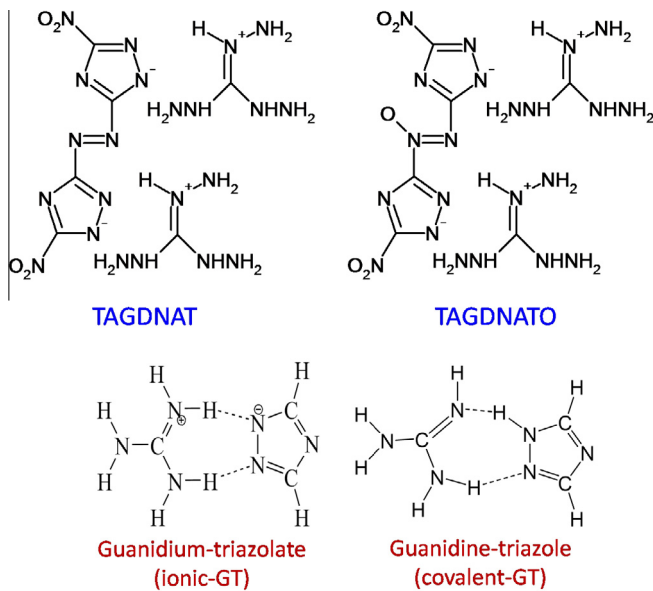


**Fig. 1.** Chemical structure of bis-triaminoguanidinium-(3,3'-dinitroazotriazolate) (TAGDNAT) and triaminoguanidium-(3,3'-dinitroazoxo-1,2,4-triazolate) (TAGDNATO), and a model system: guanidium triazolate.

Upon careful inspection of all the chemical structures given in Fig. 1, it is obvious to everybody that all guanidium triazolate-based energetic salts are nothing but organic molecules. They are decomposed under typical initiation events, such as shocks and pressure waves. Upon employing pressure using a mortar and a pestle, many organic compounds emit light flashes. This phenomenon is called triboluminescence [13] in which generation of electronically excited state species is anticipated. Many mechanisms for triboluminescence are suggested [14]; however, in general, it is well accepted that as crystal planes fracture, generation of large electric fields can electronically excite organic species. Thus, even shock waves from gentle hand grinding can excite organic molecules to the electronically excited states. These excitations are a fact and cannot be ignored in consideration of the decomposition of any energetic material. In fact, recent *ab initio* calculations show that shock compression at a pressure of 30 GPa or above can cause an electronic excitation equivalent to 2–5 eV [14e], which is comparable to the excitation energies of the low-lying excited electronic states of most of the energetic molecules. “How does such electronic excitation affect the decomposition of guanidium-triazolate-based salt?” is still an open question and no literature on the unimolecular decomposition of isolated guanidium triazolate salt following electronic excitation is found, thus far. This is why we have undertaken the task of understanding

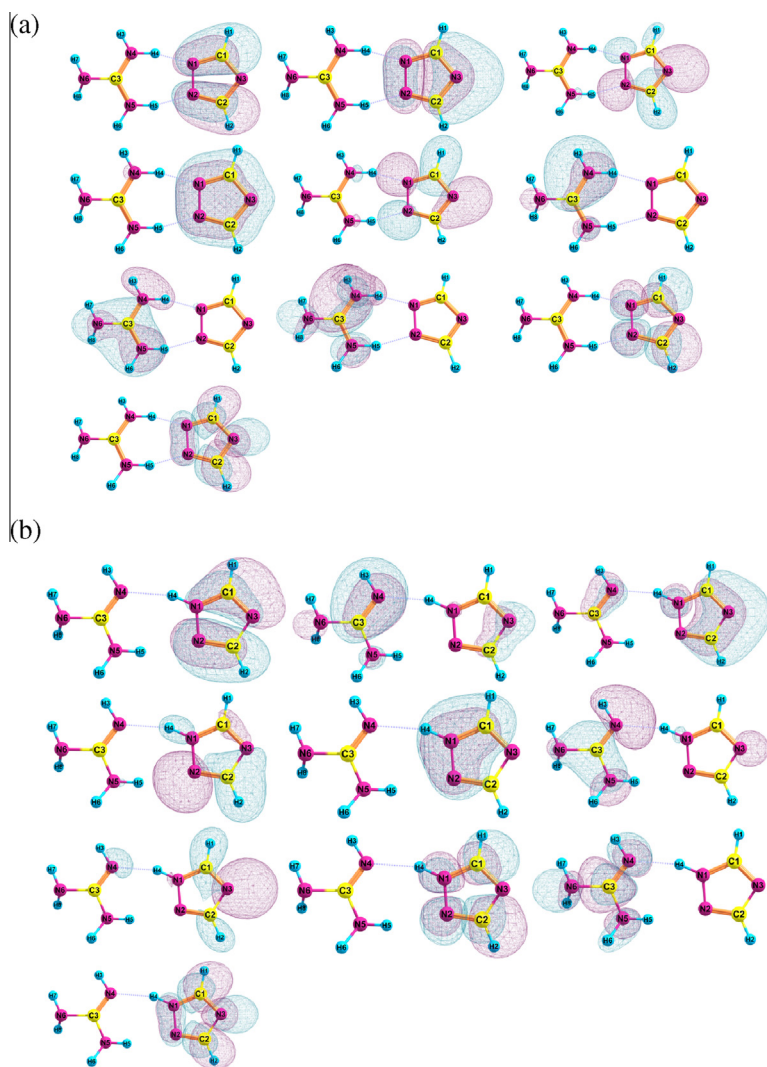


**Fig. 2.** Active orbitals used in the CASSCF, CASPT2 and CASMP2 calculations for ionic-GT (a) and covalent-GT (b).

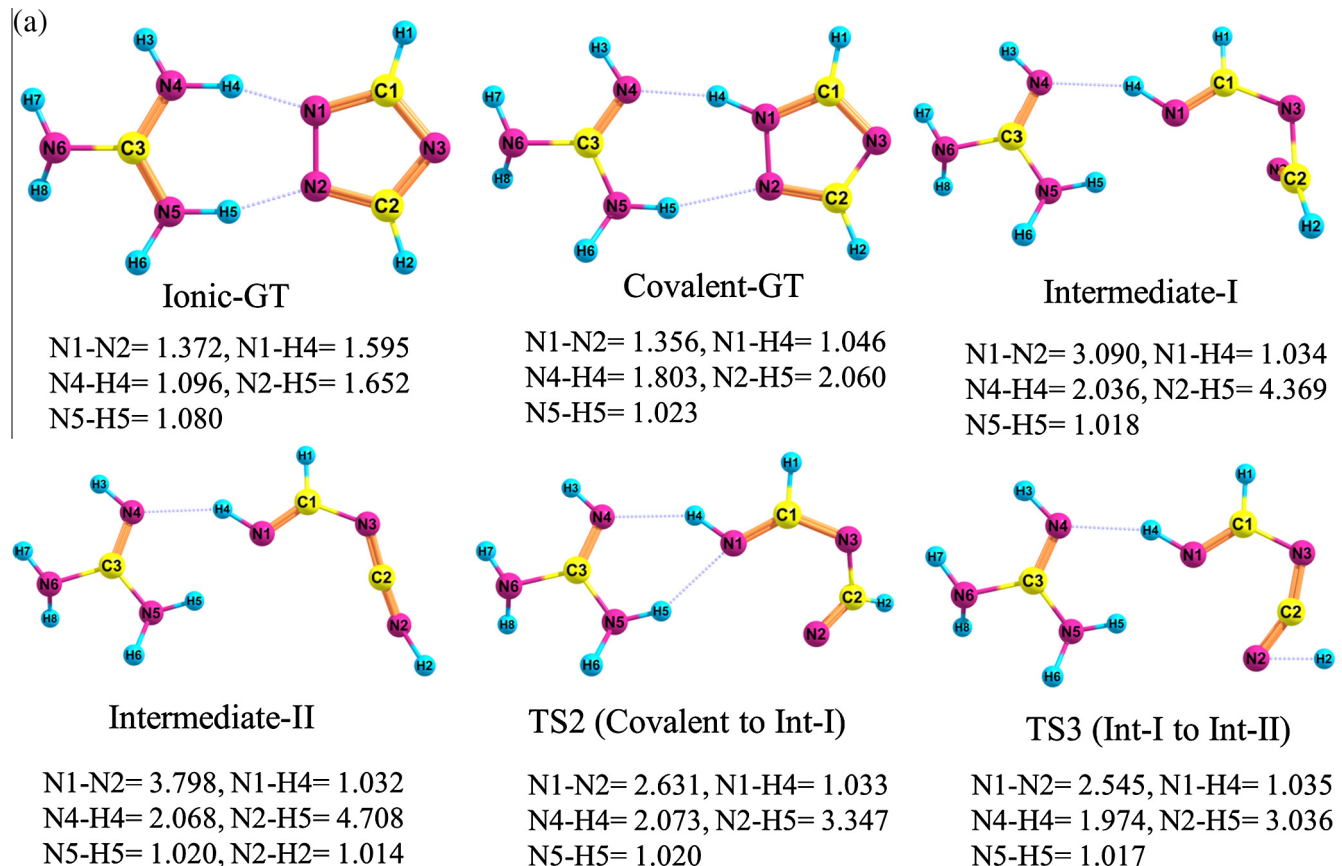


**Fig. 3.** Ground state optimized geometries of different critical points obtained at the B3LYP/6-31G(d) level of theory. Bond distances are given in Å.

unimolecular decomposition of this model salt following electronic excitation.

Our current effort is theoretical: we have performed detailed high level calculations to decipher mechanisms and reaction pathways based on the electronically excited state potential energy surfaces (PESs) that must be accessed for the chemistry to occur following electronic excitation of isolated guanidium triazolate salt. As this is an organic molecule, recent advances on theoretical organic photochemistry can serve as a well-defined and good starting point for our task. Organic molecular photochemistry is a broad and complex area, bridging many complicated molecular phenomena and interactions between different electronic PESs: [15] conical intersections (CI) which arise due to nonadiabatic coupling between two potential energy surfaces are found to play a decisive role in their chemistry following electronic excitation. In fact, recently Bhattacharya et al. has shown and firmly established, for the first time, that the conical intersections are key features which are involved in the decomposition of polyatomic energetic molecules following their electronic excitation [16]. Conical intersections provide an efficient pathway for radiationless transition between two adiabatic electronic potential energy surfaces. The probability of this nonadiabatic transition between two adiabatic surfaces becomes very high, if nuclei encounter a conical intersection, while evolving from the upper excited electronic surface to the lower one. As a result, isolated energetic molecule exhibits ultrafast nonadiabatic decomposition dynamics (taking an illustrative example, the timescale of decomposition of nitramine energetic molecules is found to be less than 100 fs [17]) through conical intersections [16(d)].

Continuing with the same theme of “role of conical intersections in nonadiabatic chemistry of energetic molecules” [16(a)], in the present work, we have explored electronically nonadiabatic processes of isolated guanidium triazolate salt, which has not been done, thus far. To the best of our knowledge, this is the first attempt to decipher the low lying electronically excited states of isolated guanidium triazolate in the gas phase. This work should serve as the foundation for further study of decomposition kinetics and dynamics of more complex guanidium triazolate-based energetic salts following electronic excitation.

## 2. Computational details

Isolated guanidium triazolate can exist in two different forms (as depicted in Fig. 1): (a) ionic form in which cationic guanidium is anchored with anionic triazolate through a double hydrogen bonding interaction, and (b) covalent form in which neutral guanidine is anchored with neutral triazole moiety through a double hydrogen bond. For simple representation, in the proceeding discussion, the first form is expressed as ionic-GT and the second form is expressed as covalent-GT.

All the geometries in the ground electronic state are optimized using both the density functional theory (DFT) with B3LYP functional and the second order Møller Plesset (MP2) perturbation theory [18] with 6-31G(d) and AUG-cc-pVTZ basis sets [19]. Stability of the optimized geometry is checked by vibrational frequency analysis at the same level of theory. Vertical excitation energies associated with the singlet excited states are calculated by

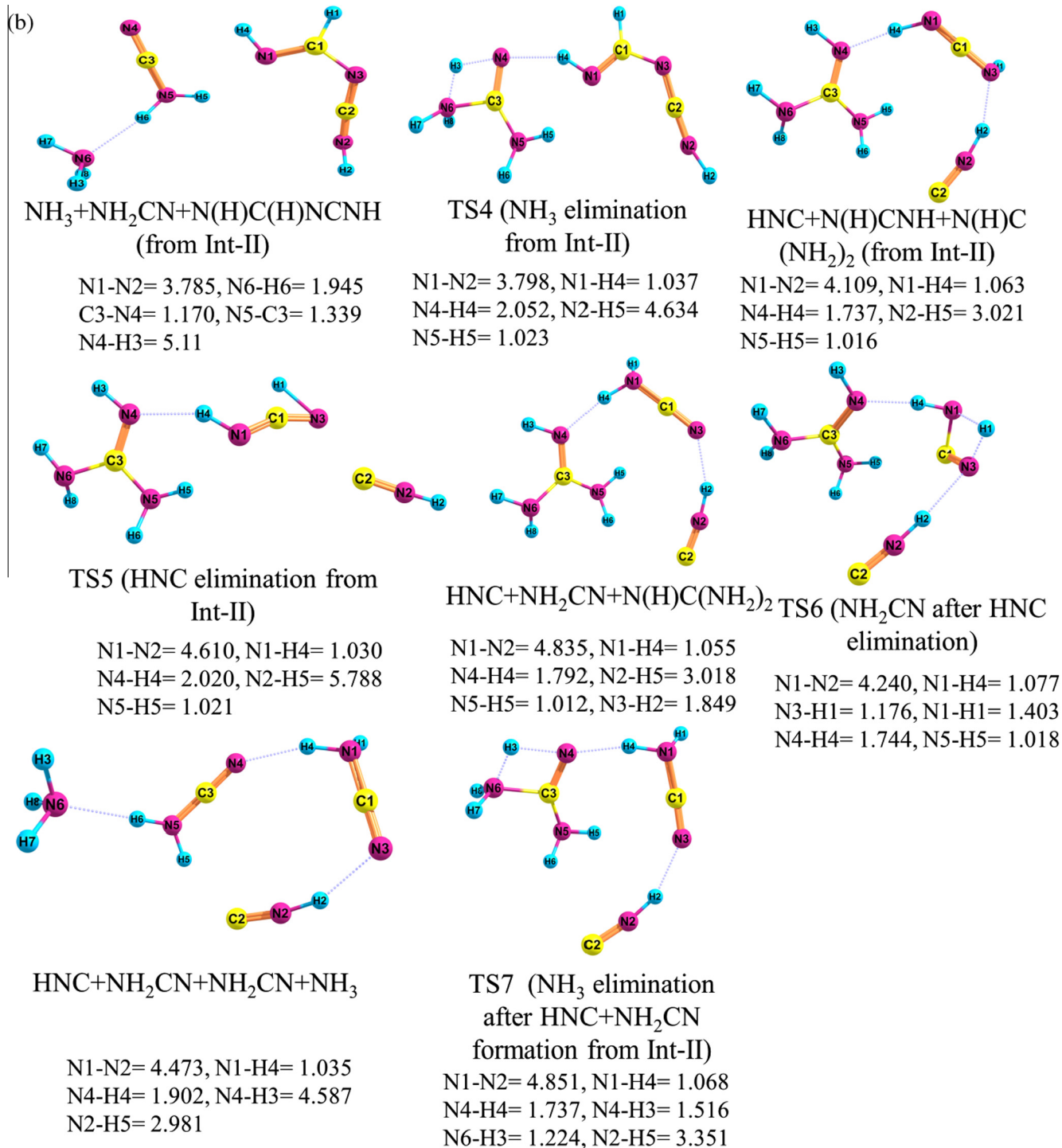


Fig. 3 (continued)

state-averaging over the ground and excited states with equal weights for each state at the complete active space self-consistent field (CASSCF) level of theory in conjunction with 6-31G(d) and AUG-cc-pVTZ basis sets. The CASSCF wave function is constructed with active space that encompasses 14 electrons and 10 valence orbitals. Active orbitals are depicted in Fig. 2 both for ionic-GT and covalent-GT. Active orbitals were selected based on the fact

that the low-lying electronically excited states of organic molecules are often found to be of  $(n, \pi^*)$  and  $(\pi, \pi^*)$  characters. That is why active space for both ionic-GT and covalent-GT includes most of the in-plane nonbonding and out-of-plane  $\pi$  and  $\pi^*$  orbitals. Search for minimum energy point on the conical intersection seam between the first excited state and the ground state surfaces is performed based on the complete active space self-consistent

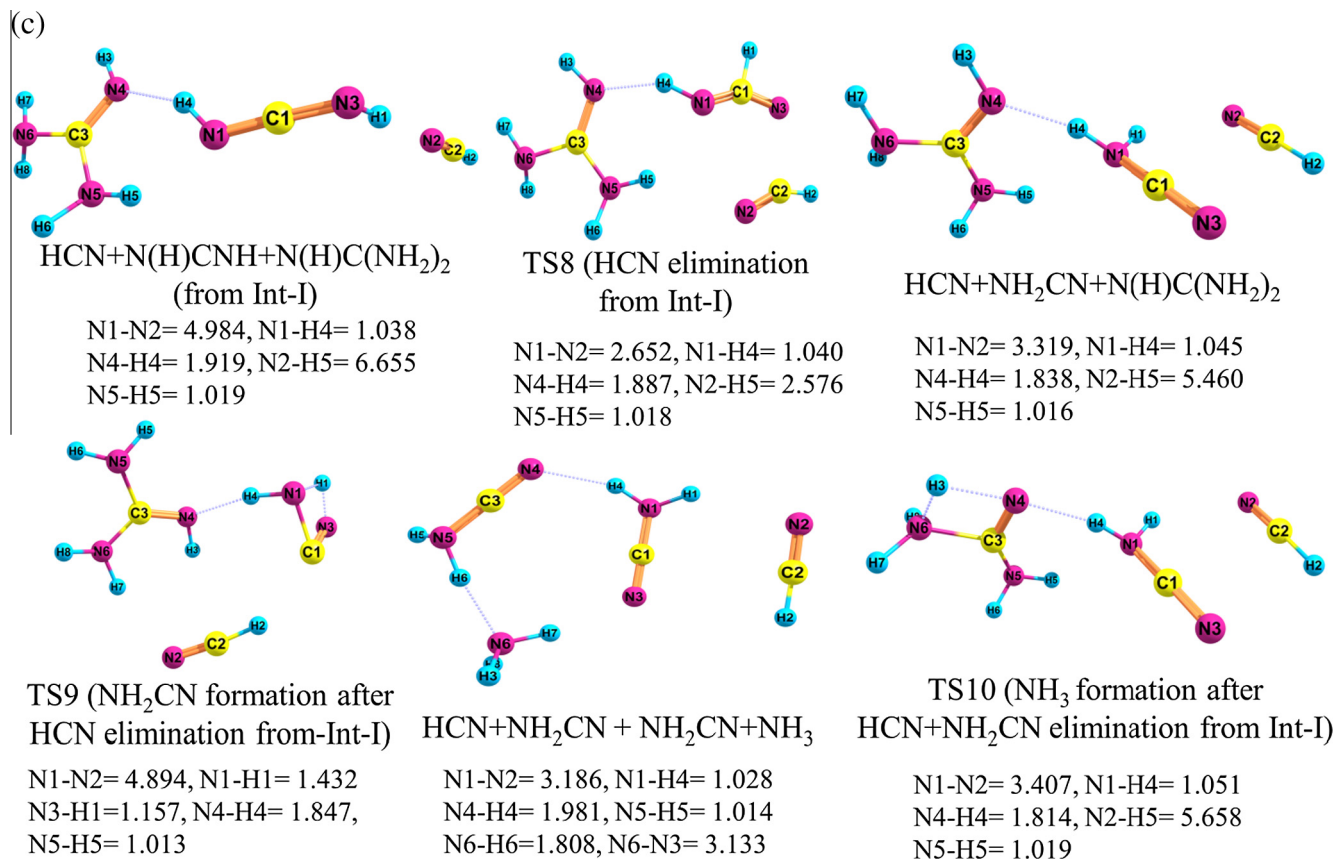


Fig. 3 (continued)

field (CASSCF) wave function using Gaussian 09 program [20]. Chemcraft [21] was used for visualization and orbital manipulation.

CASSCF calculations include only static electron-electron correlation and for accurate representation of excited electronic state surfaces, inclusion of dynamic correlation becomes often important. Complete active space second order perturbation theory can incorporate good amount dynamic correlation in addition to static correlation. That is why we have employed two methodologies: (1) complete active space second order contracted Rayleigh Schrodinger perturbation (CASPT2) theory [22] and (2) complete active space second order Møller Plesset (MP2) perturbation (CASMP2) theory [23]. The CASPT2 and CASMP2 calculations were executed using MOLPRO 2012.1 [24] and Gaussian 09 [20], respectively, using same active space (14,10) and active orbitals, as shown in Fig. 2.

Steepest decent paths (minimum energy paths) are calculated using an intrinsic reaction coordinate (IRC) algorithm implemented in Gaussian 09. If the nuclear configuration of a chemically evolving system composed of N-nuclei, then the configuration space of the chemical system is represented by 3 N cartesian coordinates. If the mass-weighted coordinate system is used then classical equation which explores potential energy surface (or reaction path) under IRC formalism is given by [25]

$$\frac{dx_1}{\left(\frac{dV}{dx_1}\right)} = \frac{dx_2}{\left(\frac{dV}{dx_2}\right)} = \dots = \frac{dx_{3N}}{\left(\frac{dV}{dx_{3N}}\right)}.$$

Thus, the IRC path represents the vibrationless-rotationless motion path of the reaction (evolving chemical system). IRC algorithm is used to explore the paths connecting the FC point of elec-

tronically excited state to the conical intersection and further to the reactants or products. As an IRC calculation requires initial force constant which can only be calculated using only 8 active orbitals using Gaussian 09, IRC calculations at the CASSCF level of theory is performed using a reduced (10,7) active space, which is shown in [Supplementary Data](#). Some of the reaction pathways of ionic-GT or covalent-GT are also explored through potential energy scanning. A relax potential energy scan is performed using Cartesian co-ordinate by changing the scan variable (respective bond distance).

### 3. Results and discussion

#### 3.1. Structure of Ionic-GT and Covalent-GT

In order to optimize ionic-GT, we placed guanidium moiety at different binding sites of triazolate moiety. The most stable geometry of ionic-GT (referred as S<sub>0,ion,Min</sub>), optimized at the B3LYP/6-31G(d) level of theory, as illustrated in Fig. 3(a), shows nearly planar structure, in which both guanidium cation and triazolate anion are bound by a strong double hydrogen bond. The N1 ··· H4 and N2 ··· H5 hydrogen bond distances are found to be 1.595 and 1.652 Å, respectively, in ionic-GT. Respective MP2- and CASSCF-results are presented in Fig. 4(a) and Fig. 5, respectively. The N1 ··· H4 and N2 ··· H5 hydrogen bond distances are predicted to be 1.623 and 1.678 Å, respectively, at the MP2 level of theory. The CASSCF level of theory estimates 1.755 and 1.754 Å, respectively.

The most stable structure of covalent-GT, optimized at the B3LYP/6-31G(d) level of theory, also exhibits a double hydrogen

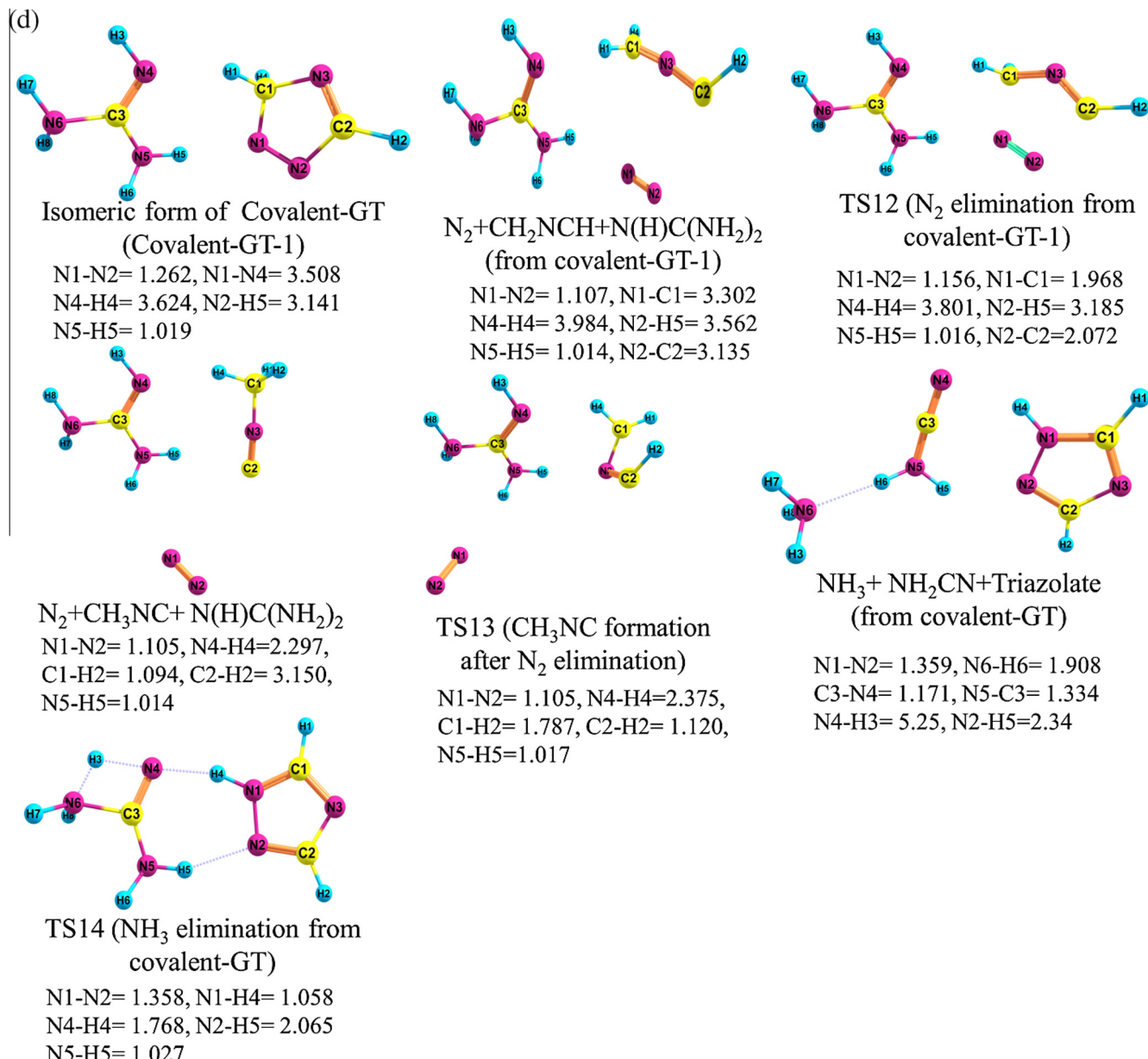


Fig. 3 (continued)

bond, as illustrated in Fig. 3(a). The N4...H4 and N2...H5 hydrogen bond distances are calculated to be 1.803 and 2.060 Å, respectively (MP2 predicts 1.821 and 2.089 Å, respectively, and CASSCF estimates 1.961 and 2.266 Å, respectively). In isolated gas phase, covalent-GT is found to be more stable than ionic-GT. The zero-point corrected electronic energy difference between covalent-GT and ionic-GT is estimated to be 7.15 kcal/mol at the B3LYP/AUG-cc-pVTZ level of theory (MP2/AUG-cc-pVTZ and CASPT2/6-31G(d) predict 6.45 and 8.30 kcal/mol, respectively, for the same). The activation barrier for the conversion of ionic-GT to covalent-GT, which occurs through one intermolecular proton transfer from guanidium to triazolate moiety, is calculated to be 0.046 kcal/mol at the B3LYP level of theory (MP2 predicts 0.46 kcal/mol).

### 3.2. Vertical excitation

MP2 and DFT (with B3LYP functional) are essentially monoconfigurational methods (i.e., they produce only adiabatic ground

electronic state surface) and therefore, they are blind to the electronically excited states. In this regard, multiconfigurational methodology, e.g., complete active space self-consistent field (CASSCF) theory is essential. This is why electronically excited state potential energy surfaces are computed at the CASSCF level of theory. For reliable estimation (by including both static and dynamic correlation) of excited state energies, complete active space second order perturbation theory is also employed.

**Ionic-GT:** Computational results obtained at the CASPT2 (14,10)/6-31G(d) level of theory show that the lowest-lying excited electronic state ( $S_1$ ) of ionic-GT has vertical excitation energy of 6.82 eV. The vertical excitation from the  $S_0$  state to the  $S_1$  state corresponds to a ( $\pi-\pi^*$ ) electronic transition. This transition is purely localized on triazolate moiety of ionic-GT. The CASMP2 level of theory, on the other hand, predicts that the  $S_1$  excited state of ionic-GT exhibits vertical excitation energy of 5.66 eV. Vertical excitation energies and excitation characters associated with other excited states ( $S_2$  and  $S_3$ ) of ionic-GT are shown in Table 1a.

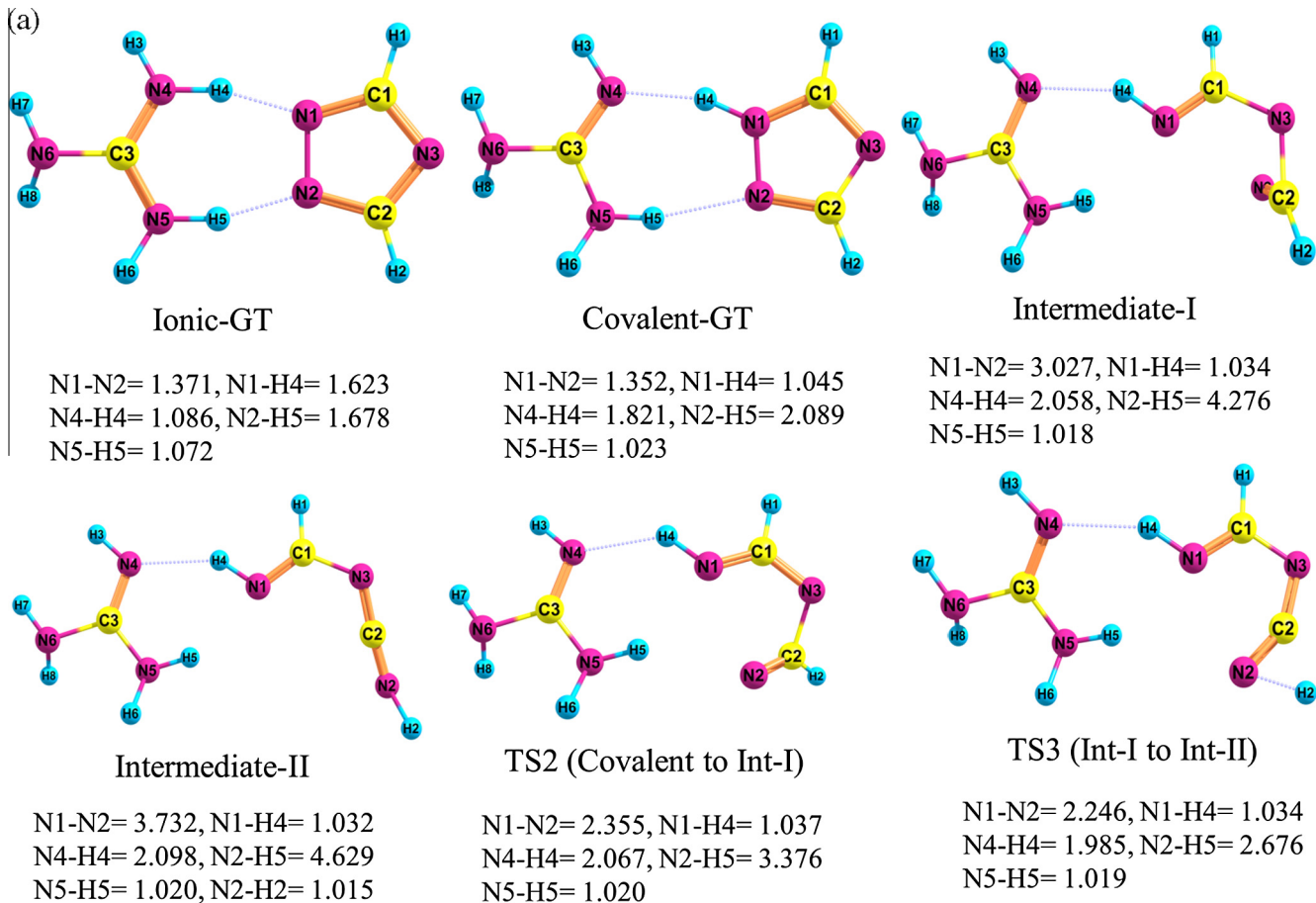


Fig. 4. Ground state optimized geometries of different critical points obtained at the MP2/6-31G(d) level of theory. Bond distances are given in Å.

**Covalent-GT:** The lowest-lying excited state ( $S_1$ ) of covalent-GT possesses vertical excitation energy of 6.82 eV, as revealed at the CASPT2(14,10)/6-31G(d) level of theory. As experimental absorption spectrum of GT (either in ionic or covalent form) is unavailable, here we compare theoretical results of covalent-GT qualitatively with experimentally obtained ultraviolet-vacuum ultraviolet (UV-VUV) absorption spectrum of structurally similar molecule N-methyl-1,2,4-triazole [26], assuming the fact that as long as the electronic excitation is localized in a single moiety of the hydrogen bonded cluster, the electronic excitation character should resemble with that of monomer.

The vertical excitation energies as well as electronic excitation characters associated with low-lying excited state ( $S_1$ ,  $S_2$ , and  $S_3$ ) of covalent-GT, computed at the CASSCF, CASPT2 and CASMP2 levels of theory, are listed in Table 1a. This table shows that two lowest-lying excited electronic states ( $S_1$  and  $S_2$ ) for covalent-GT possess vertical excitation energies of 6.82 and 7.23 eV, respectively (this result is obtained at the CASPT2 level; whereas CASMP2 predicts 5.58 and 6.46 eV, respectively) and that they both are of  $(\pi, \pi^*)$  character. Experimental UV-VUV photo-absorption spectrum of N-methyl-1,2,4-triazole shows an initial onset near 5.75 eV rising to about 6.3 eV, where the UV-VUV spectrum becomes nearly a plateau extended up to 7.15 eV [26]. Quite interestingly, we note that the vertical excitation energies associated with  $S_1$  and  $S_2$  singlet excited states, computed at the CASPT2 and CASMP2 levels of theory, closely fall in this region.

Previously, multi-reference multi-root doubles and singles (MRD-CI) method was used to compute first two excited states of

N-methyl-1,2,4-triazole and they were assigned to  $(n, \pi^*)$  and  $(\pi, \pi^*)$  characters, respectively [26]. Furthermore, the vertical excitation energies for these two states were computed to be 5.94 and 6.67 eV, respectively [26]. Direct comparison of MRD-CI-results and present CASPT2 (or CASMP2) results is not possible due to structural dissimilarities between N-methyl-1,2,4-triazole and covalent-GT. Nonetheless, at the face value, we find that the CASMP2 and CASPT2-calculated vertical excitation energies associated with the  $S_1$  and  $S_2$  states of covalent-GT are in reasonably good agreement with the previous theoretical results of N-methyl-1,2,4-triazole.

### 3.3. III Electronic PESs of ionic-GT and covalent-GT

Conical intersections, which create a funnel-like topography of PESs due to the crossing of multidimensional electronic PESs, have been firmly established to be a controlling factor in the excited electronic state decomposition of isolated energetic molecules. [16(a)] A decomposition process involving conical intersections features an electronically nonadiabatic mechanism, because of involvement of more than one PES. Although the nonadiabatic chemistry of some energetic molecules has been well studied, [16(a)] the role of nonadiabatic chemistry in the excited electronic state decomposition of ionic and covalent-GT has not been studied before. Therefore, in the proceeding discussion, we provide a complete decay path for ionic and covalent-GT from their lowest-lying excited electronic states to the ground state through conical inter-

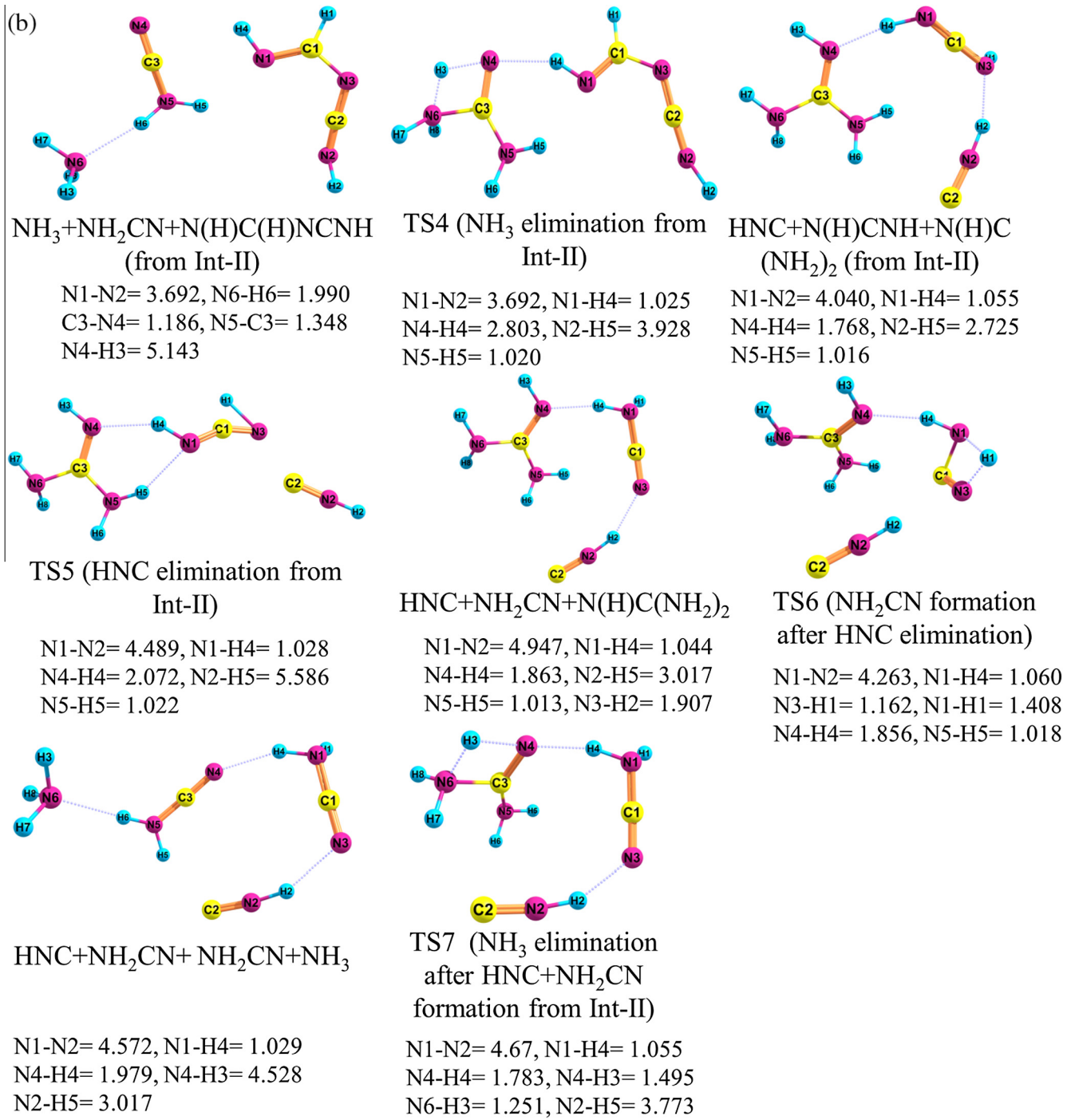


Fig. 4 (continued)

sections, explored at the CASSCF(14,10)/6-31G(d) level of theory. Two conical intersections between  $S_1$  and  $S_0$  states are optimized starting from ionic-GT and covalent-GT structures, respectively.

Minimum energy conical intersection between  $S_1$  and  $S_0$  states obtained from ionic-GT structure ( $S_{0,\text{ion}}$ ) is referred as  $(S_1/S_0)_{\text{Cl,ion}}$  and that computed from covalent-GT structure ( $S_{0,\text{cov}}$ ) is referred as  $(S_1/S_0)_{\text{Cl,cov}}$ . The optimized geometries at the  $(S_1/S_0)_{\text{Cl,ion}}$  and the  $(S_1/S_0)_{\text{Cl,cov}}$  are depicted in Fig. 5. Major differences between  $(S_1/S_0)_{\text{Cl,ion}}$  and  $(S_1/S_0)_{\text{Cl,cov}}$  geometries are found in the N–N bond distance and planarity of the triazole ring. The  $(S_1/S_0)_{\text{Cl,ion}}$  geometry exhibits an elongated N–N bond (the N1–N2 bond distance

is estimated to be 2.485 Å, as shown in Fig. 5) and possesses planar triazole moiety. On the other hand, the  $(S_1/S_0)_{\text{Cl,cov}}$  geometry exhibits a short N–N bond distance (the N1–N2 bond distance is computed to be 1.321 Å) and triazole moiety shows a nonplanar structure.

Fig. 6(a) illustrates the decay path connecting the FC point of  $S_1$  state of ionic-GT ( $S_{1,\text{FC,ion}}$ ) and the  $(S_1/S_0)_{\text{Cl,ion}}$ . These decay paths were calculated using a reduced active space in which 10 electrons are distributed in 7 active orbitals. Structural evolution along this path, which is also illustrated in Fig. 6(a), shows that this reaction path begins with N–N bond dissociation followed by excited state

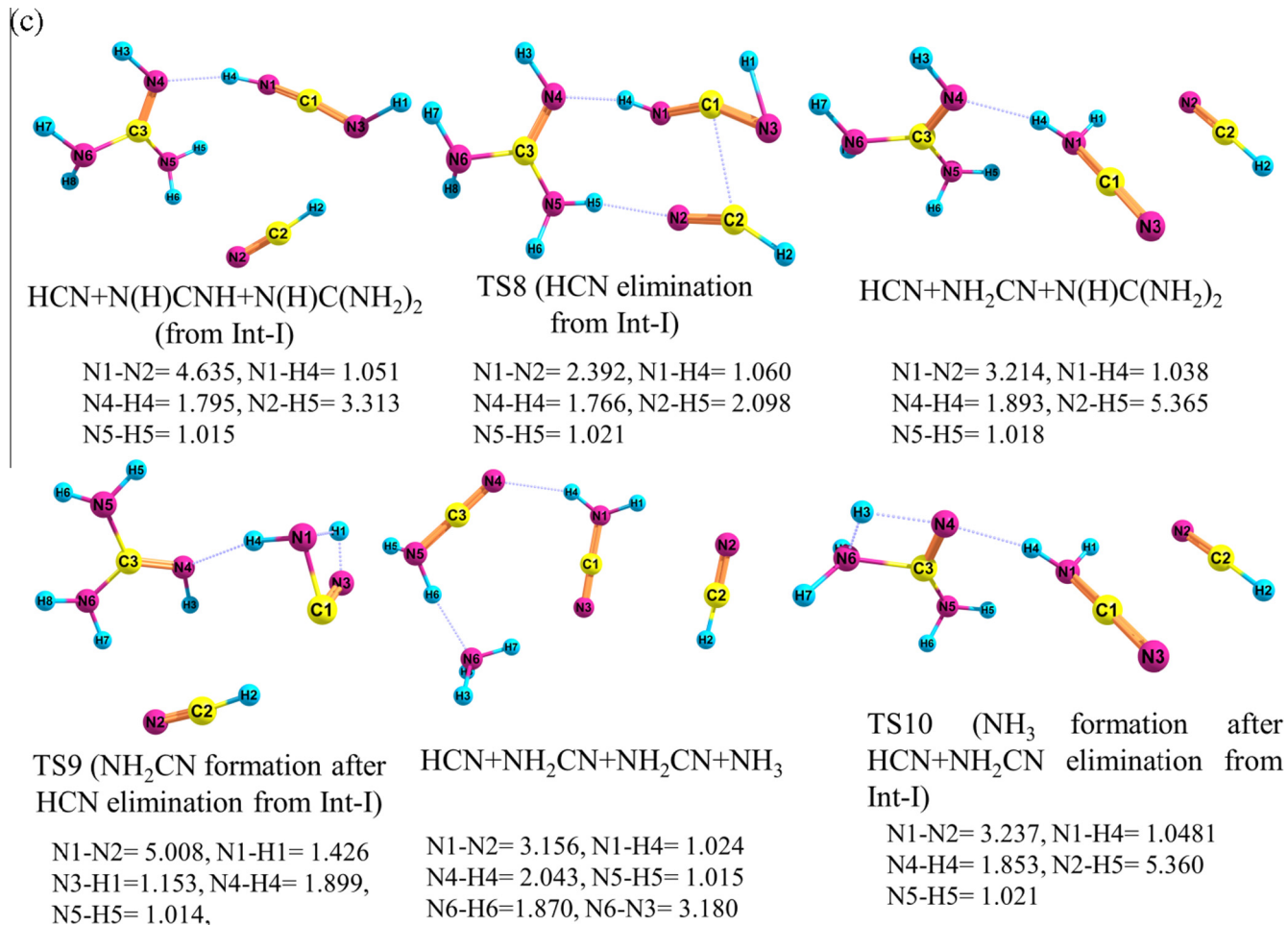


Fig. 4 (continued)

proton transfer from guanidium to triazolate moiety. On the other hand, the decay path connecting the FC point of S<sub>1</sub> state of covalent-GT ( $S_{1,FC,cov}$ ) and the ( $S_1/S_0$ )<sub>Cl,cov</sub> suggests that this excited state reaction pathway primarily eradicate planarity of the triazole ring.

A key feature of conical intersection is that more than one relaxation direction may exist on the lower electronic state surface for molecular system which is relaxing through the conical intersection from upper electronic state to the lower electronic state. This is why we have explored possible decay paths on the ground S<sub>0</sub> surface from both the ( $S_1/S_0$ )<sub>Cl,ionic</sub> and the ( $S_1/S_0$ )<sub>Cl,cov</sub> conical intersections. Fig. 6(a) shows that two minimum energy decay paths, associated with the ( $S_1/S_0$ )<sub>Cl,ionic</sub> conical intersection, on the S<sub>0</sub> ground electronic state surface exist: one connecting from ( $S_1/S_0$ )<sub>Cl,ion</sub> to the intermediate II ( $S_{0,intII}$ ) and another connecting from ( $S_1/S_0$ )<sub>Cl,ion</sub> to  $S_{0,cov}$ . On the other hand, only one decay path is obtained on the S<sub>0</sub> surface from ( $S_1/S_0$ )<sub>Cl,cov</sub>, which connects to  $S_{0,cov}$ . These paths are explicitly calculated using intrinsic reaction coordinate (IRC) algorithm implemented in Gaussian 09 [25].

Fig. 6(a) directly indicates that if ionic-GT comes back to the ground state following the ( $S_1/S_0$ )<sub>Cl,ion</sub> conical intersection, it undergoes first N–N bond dissociation, rendering triazolate ring opening on the S<sub>1</sub> excited state PES and then it undergoes proton transfer from guanidium to triazolate moiety. Finally, it follows nonadiabatic radiationless internal conversion through the ( $S_1/S_0$ )<sub>Cl,ion</sub>. The local topography of the ( $S_1/S_0$ )<sub>Cl,ion</sub>, as shown in

Fig. 6(a), exhibits a peaked conical intersection. Furthermore, the decay path connecting the FC point of S<sub>1</sub> state to the ( $S_1/S_0$ )<sub>Cl,ion</sub> on the S<sub>1</sub> surface and subsequent reaction paths, connecting the ( $S_1/S_0$ )<sub>Cl,ion</sub> and  $S_{0,cov}$  or connecting the ( $S_1/S_0$ )<sub>Cl,ion</sub> and intermediate II ( $S_{0,intII}$ ), are all predicted to be barrierless with respect to the respective FC point on the S<sub>1</sub> surface. Therefore, both covalent-GT as well as intermediate II can be produced on the ground state surface following photoexcitation of ionic-GT to the S<sub>1</sub> excited state surface.

On the contrary, when covalent-GT undergoes internal conversion through the ( $S_1/S_0$ )<sub>Cl,cov</sub>, due to presence of one decay path on the S<sub>0</sub> state surface, it converts back to the  $S_{0,cov}$  structure following its photoexcitation to the S<sub>1</sub> state. No other direct reaction pathway is obtained from the ( $S_1/S_0$ )<sub>Cl,cov</sub> conical intersection on the ground state surface. The local topography of the ( $S_1/S_0$ )<sub>Cl,cov</sub> exhibits a sloped conical intersection (see Fig. 6(b)), which suggests that covalent-GT will undergo pure internal conversion to the ground state from upper S<sub>1</sub> excited state, which finally results in vibrationally excited covalent-GT on the ground state surface.

The ring opening mechanism, which is suggested to be involved in electronically nonadiabatic chemistry of ionic-GT, can also be opened on the S<sub>0</sub> surface of ionic-GT, which can easily be explored at the MP2/6-31G(d) and B3LYP/6-31G(d) levels of theory. CASSCF calculations show that intermediate II is an important photodecomposition product of ionic-GT. This intermediate II can also be produced solely on the ground electronic potential energy surface;

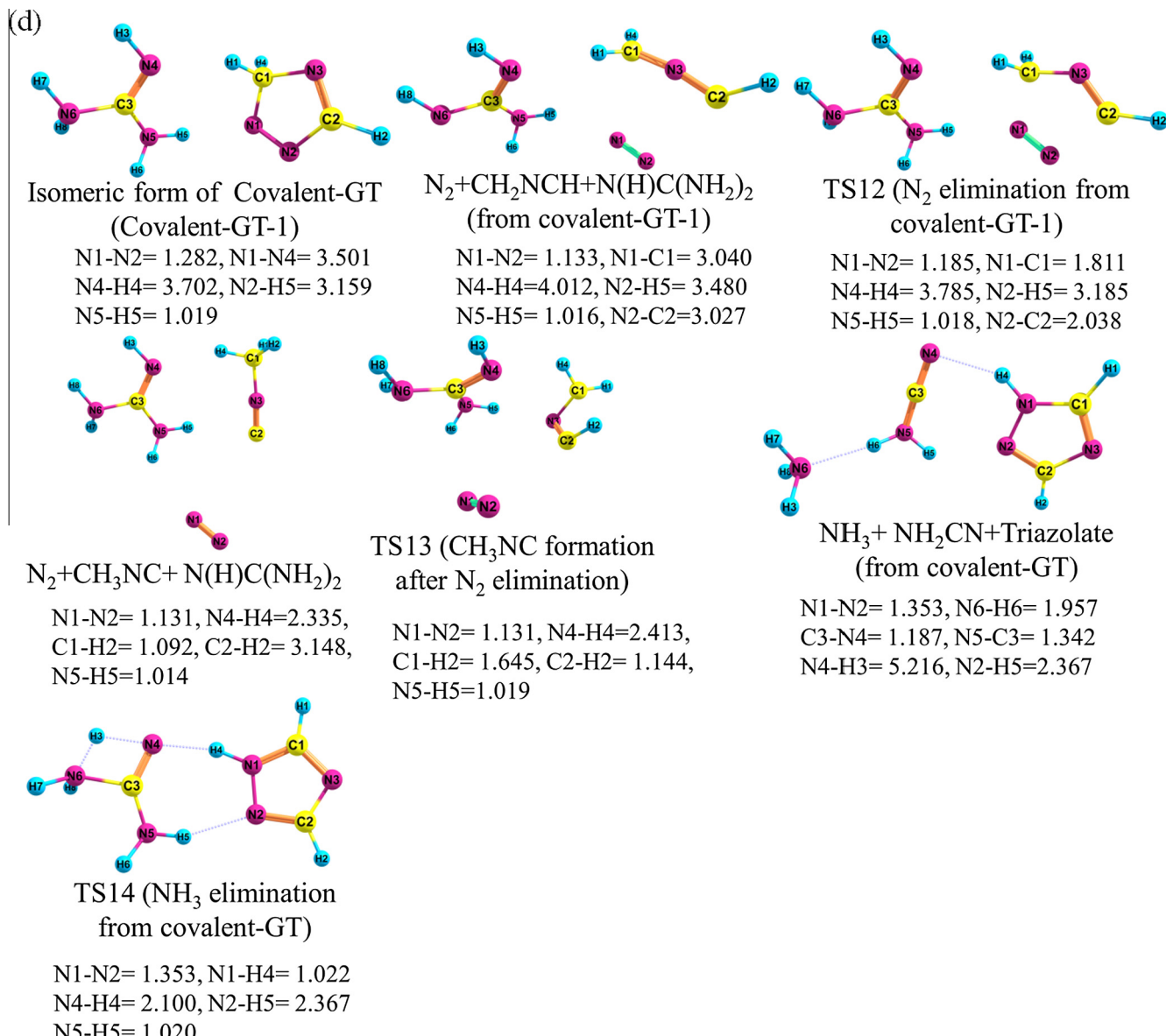


Fig. 4 (continued)

however, overall reaction path leading to intermediate II occurs through a number of steps, which are summarized in Fig. 7(a). In this process, ionic-GT is first converted to covalent-GT. Then covalent-GT undergoes N–N bond dissociation, which opens the triazole ring, rendering intermediate-I ( $S_{0,\text{int-I}}$ ). Finally, the intermediate-I undergoes hydrogen transfer, yielding intermediate-II ( $S_{0,\text{int-II}}$ ). B3LYP- and MP2-optimized structures of intermediate I and II are shown in Figs. 3(a) and 4(a), respectively. In addition, an energy profile diagram for this reaction channel, obtained at B3LYP and MP2 levels of theory is given in Fig. 7(a). Relative activation energies associated with different critical points along this pathway on the ground state surface is given in Table 2, as obtained at the MP2 and B3LYP levels of theory with 6-31G(d) and AUG-cc-pVTZ basis sets.

Both B3LYP and MP2 levels of theory predict that intermediate II is more stable than intermediate I, as evident in Table 2. This is also found at the CASSCF level of theory, as shown in Table 1b. The activation energy associated with reaction path connecting covalent-GT and intermediate I, which features mostly N–N bond

dissociation reaction channel, is estimated to be 3.79 eV at the B3LYP/6-31G(d) level of theory (the MP2/6-31G(d) predicts 4.35 eV). The activation barrier to subsequent formation of intermediate II is calculated to be 3.47 eV at the B3LYP/6-31G(d) level of theory (MP2/6-31G(d) predicts 4.02 eV). These activation barriers are calculated with respect to the  $S_{0,\text{ionic}}$  (optimized ionic-GT) energy. Improving the basis set from 6-31G(d) to AUG-cc-pVDZ does not change the results significantly, as evident in Table 2.

Intermediate II can be further dissociated via several decomposition steps on the ground potential energy surface. Intermediate II can produce HNC,  $NH_3$  and  $NH_2CN$  stable products following reaction scheme given in Fig. 7(b). The initial product HNC is generated via C–N bond dissociation from intermediate-II, which possesses an activation barrier of 4.54 eV, predicted at the B3LYP/6-31G(d) level of theory (5.12 eV is estimated at MP2/6-31G(d) level). Intermediate-II can also be dissociated to  $NH_3$  (with  $NH_2CN$ ) initial product. This dissociation channel exhibits an activation barrier of 3.53 eV at the B3LYP/6-31G(d) level of theory (MP2/6-31G(d) predicts 3.78 eV). Furthermore, intermediate-II can be converted

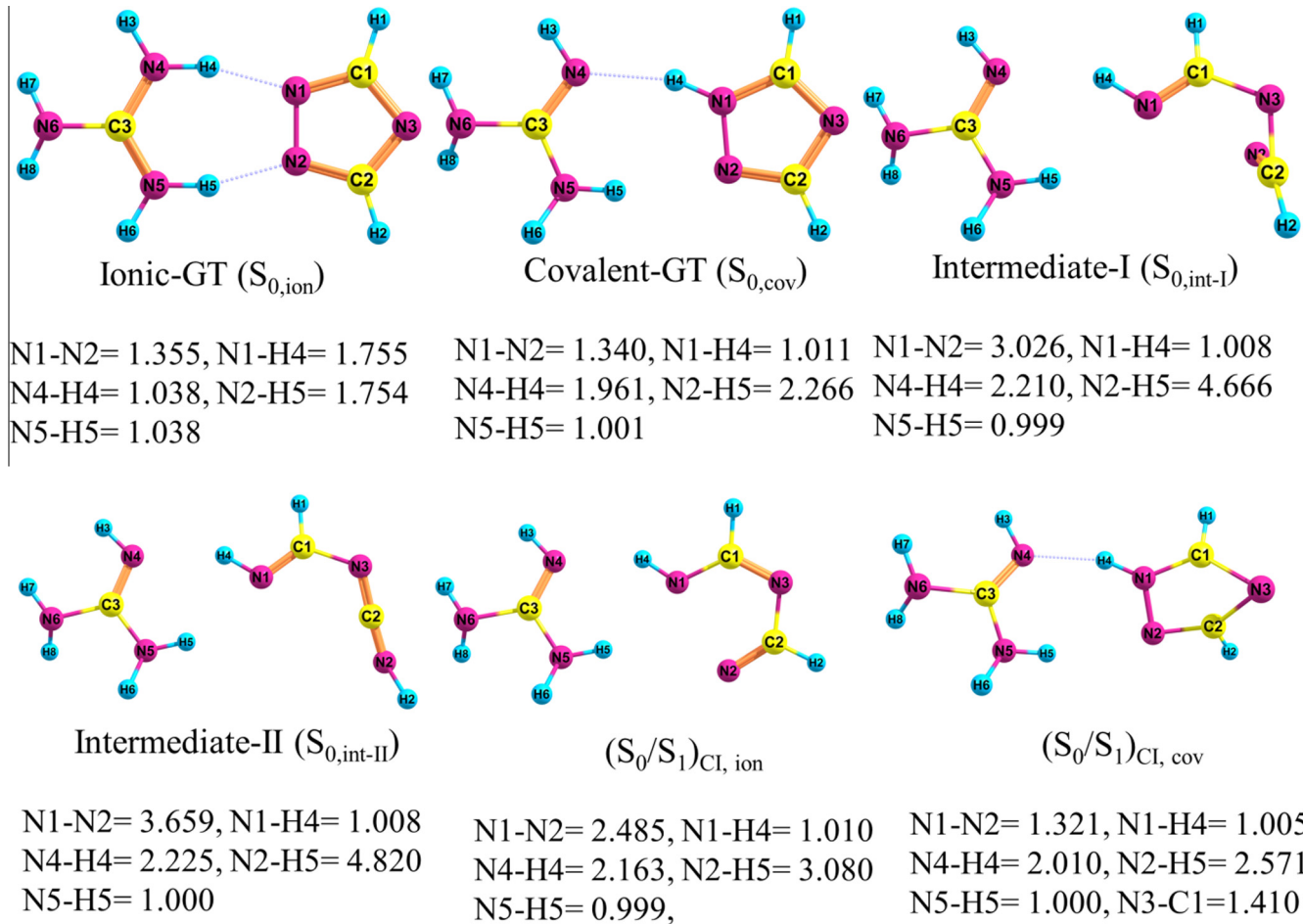


**Fig. 5.** Optimized geometries of different critical points obtained at the CASSCF(14,10)/6-31G(d) level of theory. Bond distances are given in Å.

**Table 1a**

Vertical excitation energies (in eV) and excitation characters of ionic-GT and covalent-GT computed at the CASSCF(14,10)/6-31G(d), CASPT2(14,10)/6-31G(d), CASMP2(14,10)/6-31G(d) levels of theory.

System	State	Character	Vertical excitation energy (eV) CASSCF(14,10)/6-31G(d)	Vertical excitation energy (eV) CASPT2(14,10)/6-31G(d)	Vertical excitation energy (eV) CASMP2(14,10)/6-31G(d)
Ionic-GT	$S_1$	$(\pi, \pi^*)$	7.7	6.82	5.66
	$S_2$	$(\pi, \pi^*)$	8.66	7.07	6.47
	$S_3$	$(\pi, \pi^*)$	10.05	7.79	7.33
Covalent-GT	$S_1$	$(\pi, \pi^*)$	7.40	6.82	5.58
	$S_2$	$(\pi, \pi^*)$	9.20	7.23	6.46
	$S_3$	$(\pi, \pi^*)$	10.35	8.10	7.45

to intermediate I with an activation barrier of 3.47 eV, predicted at the B3LYP/6-31G(d) level of theory (the MP2/6-31G(d) estimates 4.02 eV). The intermediate-I can subsequently be dissociated to initial HCN product, as shown in Fig. 7(c). The activation barrier associated with initial HCN elimination from intermediate-I is calculated to be 4.27 eV at the B3LYP/6-31G(d) level of theory (MP2/6-31G(d) estimates 4.12 eV). Therefore, both the MP2 and B3LYP levels of theory corroborate the fact that generation of initial NH<sub>3</sub> product (accompanied by generation of NH<sub>2</sub>CN) from intermediate-II is associated with the lowest activation barrier as compared to initial HCN or HNC generation.

Electronically ground state covalent-GT is also predicted to be one of the products which can be obtained following nonadiabatic

relaxation of ionic-GT from upper  $S_1$  state surface to the  $S_0$  ground state surface (predicted at the CASSCF level of theory and shown in Fig. 6). That is why we have also explored decomposition pathways of covalent-GT on the ground state surface. Undoubtedly covalent-GT can produce intermediate I and II and can finally render HCN, HNC, NH<sub>2</sub>CN and NH<sub>3</sub> products, following the pathways discussed above (also depicted in Fig. 7(a)–(c)). In addition to these decomposition routes, covalent-GT can also produce initial product N<sub>2</sub>, as illustrated in Fig. 7(d). In this process, covalent-GT is first converted to another covalent isomer, which subsequently dissociate to N<sub>2</sub>. The N<sub>2</sub> elimination pathway from the covalent isomer possesses an activation energy barrier of 2.34 eV, predicted at the B3LYP/6-31G(d) level of theory (the MP2/6-31G(d) estimates

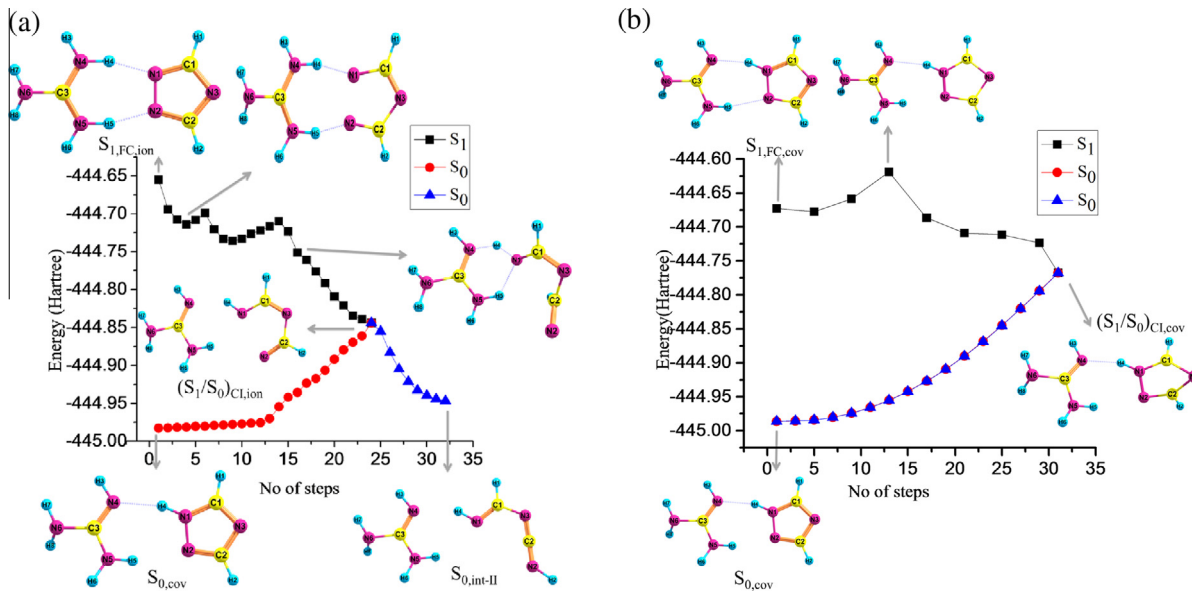


**Fig. 6.** IRC-nonadiabatic-decay path, computed at the CASSCF(10,7)/6-31G(d) level of theory for ionic-GT (a) and covalent-GT (b).

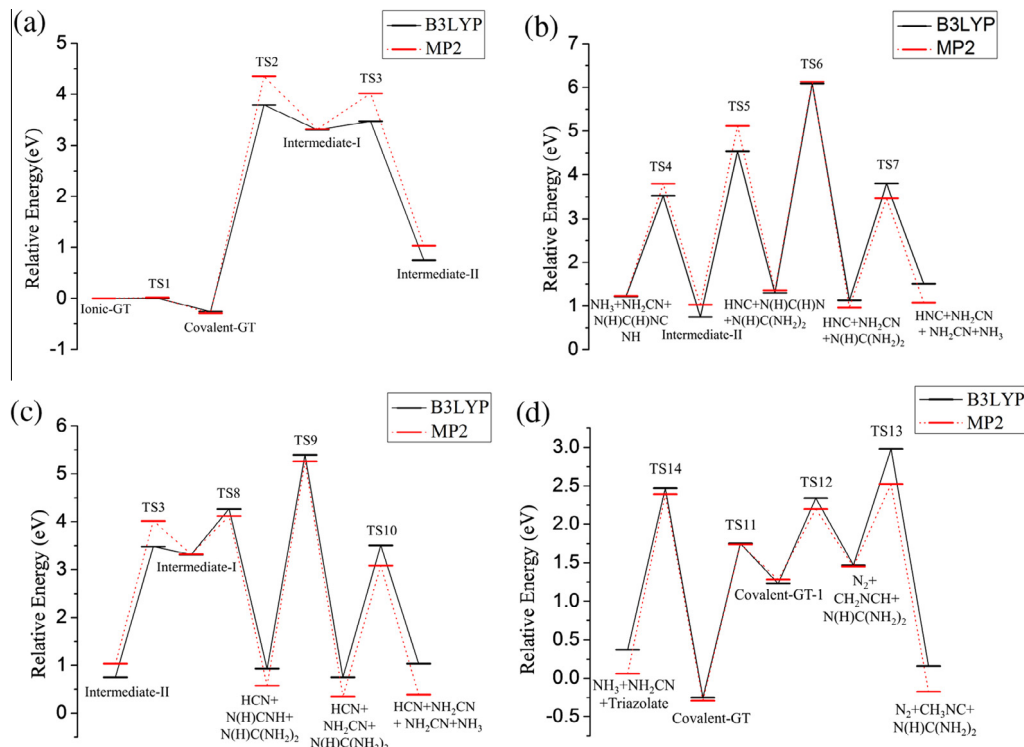


**Fig. 7.** Energy profile diagrams for (a) formation of intermediate-I and II, (b) decomposition of intermediate-II, (c) decomposition of intermediate-I, (d) decomposition of covalent-GT, computed both at the B3LYP/6-31G(d) and the MP2/6-31G(d) levels of theory.

**Table 1b**

Relative energies ( $\Delta E$  in eV) of different critical points, calculated relative to ionic-GT energy, computed at the CASSCF(14,10)/6-31G(d), CASSCF(14,10)/AUG-cc-pVTZ, CASPT2(14,10)/6-31G(d) and CASMP2(14,10)/6-31G(d) levels of theory.

Critical points	$\Delta E$ (eV) CASSCF(14,10)/6-31G(d)	$\Delta E$ (eV) CASSCF(14,10)/AUG-cc-pVTZ	$\Delta E$ (eV) CASPT2(14,10)/6-31G(d)	$\Delta E$ (eV) CASMP2(14,10)/6-31G(d)
$S_{1,FC,ion}$	7.7	7.45	6.82	5.66
$(S_0/S_1)_{Cl,ion}$	3.11	2.88	3.56	3.10
$S_{0,cov}$	-0.80	-0.75	-0.36	-1.29
$S_{1,FC,cov}$	6.6	6.7	6.46	4.29
$(S_0/S_1)_{Cl,cov}$	4.23	4.21	5.06	4.60
Intermediate-I ( $S_{0,int-I}$ )	5.15	5.06	3.33	1.72
Intermediate-II ( $S_{0,int-II}$ )	2.35	2.09	1.04	0.934

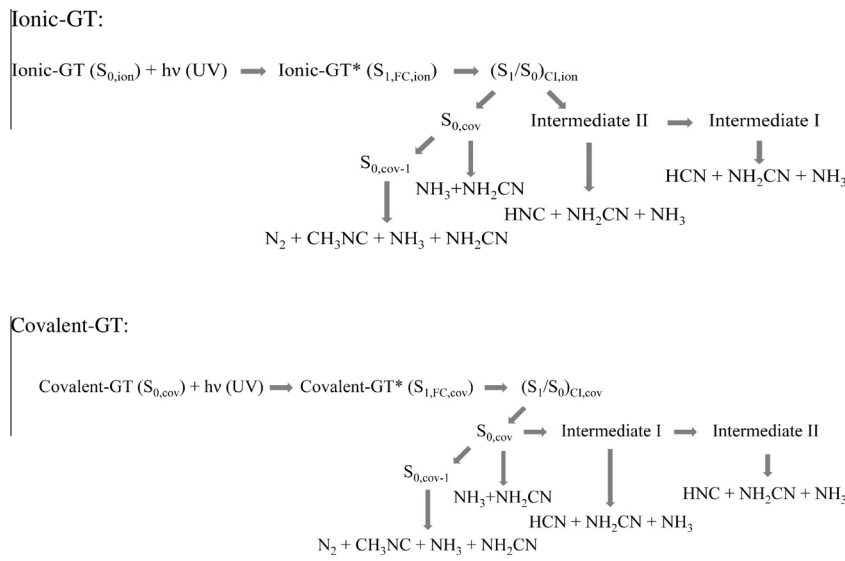
**Table 2**

Relative energies ( $\Delta E$  in eV) of different critical points, calculated relative to ionic-GT energy, computed at the B3LYP/6-31G(d), MP2/6-31G(d), B3LYP/AUG-cc-pVTZ and MP2/AUG-cc-pVTZ levels of theory.

Critical points	Figures	$\Delta E$ (eV) B3LYP/6-31G(d)	$\Delta E$ (eV) MP2/6-31G(d)	$\Delta E$ (eV) B3LYP/AUG-cc-pVTZ	$\Delta E$ (eV) MP2/AUG-cc-pVTZ
Ionic-GT ( $S_{0,\text{ion}}$ )	Figs. 3a and 4a	0.0	0.0	0.0	0.0
Covalent-GT ( $S_{0,\text{cov}}$ )		-0.25	-0.29	-0.31	-0.28
Intermediate-I ( $S_{0,\text{Int-I}}$ )		3.31	3.32	3.32	3.50
Intermediate-II ( $S_{0,\text{Int-II}}$ )		0.75	1.03	0.52	0.99
TS2 (Covalent-GT to Int-I)		3.79	4.348	3.83	4.51
TS3 (Int-I to Int-II)		3.47	4.02	3.46	4.06
$\text{NH}_3 + \text{NH}_2\text{CN} + \text{N}(\text{H})\text{C}(\text{H})\text{NCNH}$ (from Int-II)	Figs. 3b and 4b	1.22	1.225	1.06	1.48
TS4 ( $\text{NH}_3$ -elimination from Int-II)		3.53	3.785	3.51	3.89
$\text{HNC} + \text{N}(\text{H})\text{CNH} + \text{N}(\text{H})\text{C}(\text{NH}_2)_2$ (from Int-II)		1.302	1.358	1.03	1.42
TS5 (HNC-elimination from Int-II)		4.54	5.122	4.44	5.20
$\text{HNC} + \text{NH}_2\text{CN} + \text{N}(\text{H})\text{C}(\text{NH}_2)_2$ (after HNC elimination from Int-II)		1.13	0.964	0.86	1.08
TS6 ( $\text{NH}_2\text{CN}$ formation after HNC elimination from Int-II)		6.086	6.13	4.69	6.33
$\text{HNC} + \text{NH}_2\text{CN} + \text{NH}_2\text{CN} + \text{NH}_3$		1.506	1.082	1.315	1.50
TS7 ( $\text{NH}_3$ elimination after HNC + $\text{NH}_2\text{CN}$ formation from Int-II)		3.80	3.473	3.73	3.70
$\text{HCN} + \text{N}(\text{H})\text{CNH} + \text{N}(\text{H})\text{C}(\text{NH}_2)_2$ (after HCN elimination from Int-I)	Figs. 3c and 4c	0.928	0.573	0.69	0.762
TS8 (HCN elimination from Int-I)		4.27	4.12	4.2	4.24
$\text{HCN} + \text{NH}_2\text{CN} + \text{N}(\text{H})\text{C}(\text{NH}_2)_2$ (after HCN elimination)		0.75	0.346	0.56	0.628
TS9 ( $\text{NH}_2\text{CN}$ formation after HCN elimination from Int-I)		5.395	5.256	5.50	5.59
$\text{HCN} + \text{NH}_2\text{CN} + \text{NH}_2\text{CN} + \text{NH}_3$ formation		1.03	0.386	0.94	0.93
TS10 ( $\text{NH}_3$ formation after HCN + $\text{NH}_2\text{CN}$ elimination from Int-I)		3.51	3.08	3.53	3.50
Isomeric form of Covalent-GT (Covalent-GT-1)	Figs. 3d and 4	1.226	1.282	1.35	1.52
$\text{N}_2 + \text{CH}_2\text{NCH} + \text{NHC}(\text{NH}_2)_2$ (from covalent-GT-1)		1.467	1.453	1.47	1.88
TS12 ( $\text{N}_2$ elimination from Covalent-GT-1)		2.335	2.20	2.46	2.49
$\text{N}_2 + \text{CH}_3\text{NC} + \text{N}(\text{H})\text{C}(\text{NH}_2)_2$ (after $\text{N}_2$ elimination)		0.159	-0.174	0.165	0.35
TS13 (formation of $\text{CH}_3\text{NC}$ after $\text{N}_2$ elimination)		2.980	2.52	3.12	3.06
$\text{NH}_3 + \text{NH}_2\text{CN} + \text{Triazolate}$ from covalent-GT		0.37	0.06	0.38	0.336
TS14 ( $\text{NH}_3$ elimination from Covalent-GT)		2.47	2.39	2.62	2.53

2.20 eV). Furthermore, covalent-GT can directly dissociate to initial  $\text{NH}_3$  product (accompanied by generation of  $\text{NH}_2\text{CN}$ ) and this pathway exhibits an activation barrier of 2.47 eV which is predicted at the B3LYP/6-31G(d) level of theory (the MP2/6-31G(d) estimates 2.39 eV).

AUG-cc-pVTZ basis sets. Several possible electronically nonadiabatic reaction pathways for ionic-GT and covalent-GT are proposed from their  $S_1$  excited states, which are summarized below:



#### 4. Summary and conclusions

In the present computational study, decomposition of isolated electronically excited ionic-GT and covalent-GT has been investigated utilizing the CASSCF, CASPT2, CASMP2, MP2 and DFT (with B3LYP functional) levels of theory with 6-31G(d) and

Under isolated gas phase conditions, following electronically nonadiabatic transition from the upper  $S_1$  excited state surface to the lower ground state surface through the conical intersection, whole electronic excitation energy, associated with the vertical

excitation to the  $S_1$  state, is finally stored in vibrational degrees of freedom on the ground potential energy surface. Therefore, if ionic-GT undergoes nonadiabatic relaxation from the upper electronic state to the lower electronic state through the  $(S_1/S_0)_{\text{Cl,ion}}$ , this cluster, finally stores approximately 6.82 eV (predicted at the CASPT2 level; 5.66 eV was predicted by CASMP2) energy in vibrational degrees of freedom of covalent-GT and intermediate II (as both are predicted to be generated following photoexcitation of ionic-GT). Similarly, when covalent-GT undergoes electronically nonadiabatic transition from the upper electronic state to the ground state through the  $(S_1/S_0)_{\text{Cl,cov}}$ , it produces vibrationally excited covalent-GT on the ground potential energy surface. Consequently, in principle,  $\text{N}_2$ ,  $\text{HCN}$ ,  $\text{HNC}$ ,  $\text{NH}_3$ ,  $\text{NH}_2\text{CN}$  and  $\text{CH}_3\text{NC}$  products can be produced if available internal energy is enough to circumvent the respective activation barriers (given in Table 2 and depicted in Fig. 7). However, it is evident in all the energy profile diagrams in Fig. 7, that both  $\text{N}_2$  elimination and  $\text{NH}_3$  elimination (accompanied by generation of  $\text{NH}_2\text{CN}$ ) reaction steps possess the lowest activation barriers. Here, we note that  $\text{N}_2$  elimination occurs on an isomeric form of triazole moiety and  $\text{NH}_3$  elimination (accompanied by generation of  $\text{NH}_2\text{CN}$ ) occurs on the guanidine moiety.

Therefore, present theoretical calculation predicts that decomposition product formation from ionic-GT and covalent-GT occurs only on the electronically ground  $S_0$  PES with high vibrational excitation after nonadiabatic evolution of the respective cluster through the conical intersection from  $S_1$  excited state. Both  $\text{N}_2$  and  $\text{NH}_3$  (with  $\text{NH}_2\text{CN}$ ) products are predicted to be the major initial decomposition products from ionic-GT and covalent GT following their electronic excitation. Furthermore, inter-conversion between ionic-GT and covalent-GT is energetically feasible during electronically nonadiabatic relaxation from upper excited state to the lower ground electronic state. Undoubtedly, to confirm these predictions, experimental effort must be undertaken; however, the present results are consistent with general consensus that high nitrogen content energetic systems should produce  $\text{N}_2$  as their decomposition product. The  $\text{N}_2$  product is generated through ring rupture of one structural isomer of triazole generated from covalent-GT. On the other hand, the  $\text{NH}_3$  product (with  $\text{NH}_2\text{CN}$ ) is generated from guanidine moiety of covalent-GT.

## Conflict of interest

There is no conflict of interest.

## Acknowledgements

Indian Institute of Science (IISc, Part-2A-XII Plan 12-0201-0243-01-403) and ISRO-IISc Space Technology Cell (ISTC/CIP/ATB/0333) are gratefully acknowledged for the financial support of this research.

## Appendix A. Supplementary data

Supplementary data associated with this article can be found, in the online version, at <http://dx.doi.org/10.1016/j.chemphys.2015.10.016>.

## References

- [1] G. Steinhauser, T.M. Klapötke, *Angew. Chem. Int. Ed.* **47** (2008) 3330.
- [2] R.P. Singh, R.D. Verma, D.T. Meshri, J.M. Shreeve, *Angew. Chem. Int. Ed.* **45** (2006) 3584.
- [3] C. Darwich, T.M. Klapötke, C.M. Sabaté, *Chem. Eur. J.* **14** (2008) 5756.
- [4] G.W. Drake, T.W. Hawkins, A.J. Brand, L.A. Hall, M. McKay, *Propellants Explos. Pyrotech.* **28** (2003) 174.
- [5] K. Karaghiosoff, T.M. Klapötke, P. Mayer, H. Piotrowski, K. Polborn, R.L. Willer, J. Weigand, *J. Org. Chem.* **71** (2006) 1295.
- [6] H. Gao, C. Ye, O.D. Gupta, J.C. Xiao, M.A. Hiskey, B. Twamley, J.M. Shreeve, *Chem. Eur. J.* **13** (2007) 3853.
- [7] C.B. Jones, R. Haiges, T. Schroer, K.O. Christe, *Angew. Chem. Int. Ed.* **45** (2006) 4981.
- [8] A.R. Katritzky, S. Singh, K. Kirichenko, M. Smiglak, J.D. Holbrey, W.M. Reichert, S.K. Spear, R.D. Rogers, *Chem. Eur. J.* **12** (2006) 4630.
- [9] T.M. Klapötke, P. Mayer, A. Schulz, J.J. Weigand, *J. Am. Chem. Soc.* **127** (2005) 2032.
- [10] Z. Zeng, H. Gao, B. Twamley, J.M. Shreeve, *J. Mater. Chem.* **17** (2007) 3819.
- [11] G.H. Tao, Y. Guo, Y.H. Joo, B. Twamley, J.M. Shreeve, *J. Mater. Chem.* **18** (2008) 5524.
- [12] (a) H. Gao, C. Ye, C.M. PiekarSKI, M. Shreeve, *J. Phys. Chem. C* **111** (2007) 10718;  
 (b) D.E. Chavez, B.C. Tappan, B.A. Mason, *Propellants Explos. Pyrotech.* **34** (2009) 475;  
 (c) G. Drake, T. Hawkins, A. Brand, L. Hall, M. McKay, A. Vij, I. Ismail, *Propellant Explos. Pyrotech.* **28** (2003) 174.
- [13] (a) H.M. Windawi, S.P. Varma, C.B. Cooper, F. Williams, *J. Appl. Phys.* **47** (1976) 3418;  
 (b) J. Schanda, B. Baron, F. Williams, *J. Lumin.* **9** (1974) 338;  
 (c) S.P. Varma, F. Williams, *J. Chem. Phys.* **59** (1973) 912;  
 (d) F. Williams, *Adv. Chem. Phys.* **21** (1971) 289;  
 (e) J. Sharma, J.W. Forbes, C.S. Coffey, T.P. Liddiard, *J. Phys. Chem.* **91** (1987) 5139–5144;  
 (f) J. Sharma, B.C. Beard, M. Chaykovsky, *J. Phys. Chem.* **95** (1991) 1209–1213;  
 (g) Z.A. Dreger, Y.A. Grusdkov, Y.M. Gupta, J.J. Dick, *J. Phys. Chem. B* **106** (2001) 247;  
 (h) Y. Tsuboi, T. Seto, N. Kitamura, *J. Phys. Chem. B* **107** (2003) 7547;  
 (i) B.P. Aduev, E.D. Aluker, M.M. Kuklja, A.B. Kunz, E.H. Younk, *J. Lumin.* **91** (2000) 41.
- [14] (a) E.J. Reed, J.D. Joannopoulos, L.E. Fried, *Phys. Rev. B* **62** (2000) 16500;  
 (b) M. Manaa, L. Fried, E. Reed, *J. Comput. Aided Mat. Des.* **10** (2003) 75;  
 (c) M.R. Manaa, L.E. Fried, *J. Phys. Chem. A* **103** (1999) 9349;  
 (d) M.M. Kuklja, E.V. Stefanovich, A.B. Kunz, *J. Chem. Phys.* **112** (2000) 3417;  
 (e) M.M. Kuklja, B.P. Aduev, E.D. Aluker, V.I. Krasheninnik, A.G. Krechetov, A.Y. Mitrofanov, *J. Appl. Phys.* **89** (2001) 4156–4166;  
 (f) M.M. Kuklja, A.B. Kunz, *J. Phys. Chem. Solids* **61** (2000) 35–44;  
 (g) A.B. Kunz, D.R. Beck, *Phys. Rev. B* **36** (1987) 7580.
- [15] (a) M. Klessinger, J. Michl, *Excited States and Photochemistry of Organic Molecules*, Wiley-VCH, New York, 1995;  
 (b) N.J. Turro, J.C. Scaiano, V. Ramamurthy, *Modern Molecular Photochemistry of Organic Molecules*, University Science Books, Sausalito, CA, 2010;  
 (c) H. Nakamura, *Nonadiabatic Transition: Concepts, Basic Theories and Applications*, World Scientific Publishing Company, New Jersey, 2012;  
 (d) M. Olivucci, *Computational Photochemistry*, Elsevier, Amsterdam, Netherlands, 2005;  
 (e) M. Baer, *Beyond Born-Oppenheimer: Electronic Nonadiabatic Coupling Terms and Conical Intersections*, John Wiley & Sons, Hoboken, New Jersey, 2006.
- [16] (a) A. Bhattacharya, Y.Q. Guo, E.R. Bernstein, *Acc. Chem. Res.* **43** (2010) 1476;  
 (b) A. Bhattacharya, Y.Q. Guo, E.R. Bernstein, *J. Phys. Chem. A* **113** (2009) 811;  
 (c) A. Bhattacharya, Y.Q. Guo, E.R. Bernstein, *J. Chem. Phys.* **131** (2009) 194304;  
 (d) A. Bhattacharya, E.R. Bernstein, *J. Phys. Chem. A* **115** (2011) 4135;  
 (e) A. Bera, A. Bhattacharya, *J. Chem. Sci.* **127** (2015) 71;  
 (f) A. Bera, S. Maroo, A. Bhattacharya, *Chem. Phys.* **446** (2015) 47.
- [17] M. Greenfield, Y.Q. Guo, E.R. Bernstein, *Chem. Phys. Lett.* **430** (2006) 277.
- [18] (a) A.D. Becke, *J. Chem. Phys.* **98** (1993) 5648;  
 (b) C. Lee, W. Yang, R.G. Parr, *Phys. Rev. B* **37** (1988) 785;  
 (c) M. Head-Gordon, J.A. Pople, M.J. Frisch, *Chem. Phys. Lett.* **153** (1988) 503.
- [19] (a) T.H. Dunning Jr., *J. Chem. Phys.* **90** (1989) 1007;  
 (b) P.S. Hariharan, J.A. Pople, *Theor. Chem. Acc.* **23** (1973) 213.
- [20] M.J. Frisch, G.W. Trucks, H.B. Schlegel, et al., *Gaussian 09*, Gaussian Inc., Pittsburgh, PA, 2009.
- [21] <<http://www.chemcraftprog.com/>>.
- [22] P. Celani, H.-J. Werner, *J. Chem. Phys.* **112** (2000) 5546.
- [23] J.J. McDouall, K. Peasley, M.A. Robb, *Chem. Phys. Lett.* **148** (1988) 183.
- [24] H.-J. Werner, P. J. Knowles, G. Knizia, F. R. Manby, M. Schütz, P. Celani, T. Korona, R. Lindh, A. Mitrushenkov, G. Rauhut, K. R. Shamasundar, T. B. Adler, R. D. Amos, A. Bernhardsson, A. Berning, D. L. Cooper, M. J. O. Deegan, A. J. Dobbyn, F. Eckert, E. Goll, C. Hampel, A. Hesselmann, G. Hetzer, T. Hrenar, G. Jansen, C. Köppel, Y. Liu, A. W. Lloyd, R. A. Mata, A. J. May, S. J. McNicholas, W. Meyer, M. E. Mura, A. Nicklass, D. P. O'Neill, P. Palmieri, D. Peng, K. Pflüger, R. Pitzer, M. Reiher, T. Shiozaki, H. Stoll, A. J. Stone, R. Tarroni, T. Thorsteinsson, M. Wang, *MOLPRO*, version 2012.1.
- [25] K. Fukui, *Acc. Chem. Res.* **14** (1981) 363.
- [26] Michael H. Palmer, Philip J. Camp, Søren Vrønning Hoffmann, Nykola C. Jones, Ashley R. Head, Dennis L. Lichtenberger, *J. Chem. Phys.* **136** (2012) 094310.